Quasi-Direct Nonprehensile Catching with Uncertain Object States*

Markus M. Schill[1,2], Felix Gruber[1], and Martin Buss[1,2]

***Abstract*— One of the key challenges in dynamic manipulation is to establish continuous contact between a moving object and a manipulator. Direct robotic catching is a benchmark in this context, especially without grasping devices. In this paper, we explain why it is unrewarding to aim for an ideal initial dynamic contact if only imprecise knowledge of the object states is available. Robust initial contacts are proposed such that a successful quasi-direct catch can be predicted. The proposed robustness originates in a negative relative acceleration between object and catching end-effector. Sets, for which an upper negative relative acceleration bound holds, are evaluated throughout an exemplary catching motion. Reachable set computations allow to express and visualize these sets of successful object states at any point in time before contact. The paper closes with a robot-robot experiment that shows successful quasi-direct catches without feedback on the object states for a robotic throw.**

I. Introduction

Dynamic and reliable manipulation is of great relevance for industrial applications or robotic sports. Solutions to growing dynamical task requirements mostly originate in more complex robotic systems that are specially developed for a particular application. If the task changes, a new robot or at least a new end-effector must be designed. In order to provide reliability, these systems are typically oversized and thus have high costs per unit.

The framework of dynamic manipulation intends to counter this development with simple robot structures that can execute dynamically complex tasks. The term dynamic manipulation was formed and discussed by Mason and Lynch [1]. They stated that task dynamics can or should be actively used to enhance the manipulation capabilities of low degree of freedom (DoF) robots. Mason and Lynch differentiate between form or force closure grasps and nonprehensile dynamic manipulation [2]. The latter term summarizes all interactions between manipulators and objects without grasping devices. Instead, generic end-effector structures are used, which reduce cost, mechanical complexity, and increase the applicability to multiple types of tasks or objects.

Within nonprehensile manipulation, the goal is to modify the states of the object making use of instantaneous and continuous contacts. Continuous contacts can be further divided into the problem of establishing and maintaining contact. Nonprehensile robotic catching is a benchmark for both subproblems, each coming with individual challenges. A successful catch typically relies on a combination of sophisticated solutions in robot control, multiple types of sensory feedback, dynamic modeling and trajectory planning. The first two components aim at improving the repeatability of a task. Since dynamic modeling implies the definition of successful contact situations, it is the foundation for planning robust catching trajectories.

In the presence of imprecise information about the object states, continuous contacts in nonprehensile catching cannot be guaranteed initially as re-bounces may occur. Hence, nonprehensile catching must not only consider the initial contact but rather the entire catching motion. For situations where a direct catch, which requires to match all states of an object at the same time instant, is not possible, indirect catches were proposed [3], [4]. These indirect catches prepare the object with an instantaneous contact such that a subsequent direct catch becomes possible. The proposed quasi-direct catch is located in between these two approaches: intentional impacts without requiring full motion prediction of the consecutive object flight.

Hove and Slotine [5] presented one of the first experiments in dynamic catching, where a robot end-effector matches position and velocity with an object. They managed to follow the flight path of an object with a robotic manipulator for a finite time. Some years later, dynamic catching was discussed in Lynch and Mason's dynamic manipulation framework [2].

However, until today, most approaches in object catching are closed-loop by means of complex vision systems. Research thus focuses on efficient image processing and flight trajectory estimation. Overcoming these challenges allows for enough time to find a robot motion that intercepts the object trajectory with a grasping manipulator [6]. Some approaches took a step further and defined the kinematic trajectory interception as an optimization problem [7]. Bäuml *et al.* [8] are even able to plan a kinematically optimal robot interception trajectory online. In all these grasping based approaches, the contact time estimation is crucial to close the gripper at the right time. They all focus on kinematic interception leading to high impact forces if both manipulator and object are not designed specifically.

Dynamic object manipulation is one possibility to reduce these high impact forces, but it demands a physical investigation of the expected contacts. They can range from the desire of keeping contact [9] to intentional impacts [3]. For nonprehensile catching, the impact model is of great importance, which is a classic research area itself with many approaches and publications. Most important for our

*This work was supported in part within the ERC Advanced Grant SHRINE Agreement No. 267877 (www.shrine-project.eu) and in part by the Technische Universität München - Institute for Advanced Study (www.tum-ias.de), funded by the German Excellence Initiative

[1]Chair of Automatic Control Engineering, Technische Universität München, Theresienstr. 90, 80333 München, Germany, {m.schill, felix.gruber, mb}@tum.de

[2]TUM Institute for Advanced Study, Technische Universität München, Lichtenbergstrasse 2a, 85748 Garching, Germany

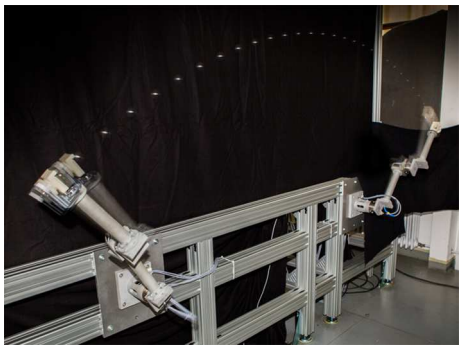

Fig. 1. Experimental setup with two symmetric 2-DoF planar robots.

work is the basic impulse-based framework introduced by Wang and Mason [10], [11] that builds on Routh's graphical approach [12]. The role of negative acceleration was first discussed by Schaal [13] for robotic juggling.

In this work, we investigate how to find sets of object states for nonprehensile catching that lead to continuous contact and thus to task success. It is explained why it is unrewarding to aim for an ideal initial dynamic contact if no precise knowledge of the object states is available. Hence, a set of successful object states is defined, based on negative relative acceleration between object and end-effector. The negative acceleration must be shown to hold after initial contact throughout the remaining catching motion. Only then, a strictly monotonically decreasing re-bounce height for any consecutive impact can be guaranteed. The sets are calculated for an exemplary catching motion to evaluate the restriction of the negative acceleration assumption.

The remainder of the paper is organized as follows. Section II simplifies the modeling process as it defines all object states and dynamics relative to the end-effector coordinate frame. Section III introduces a bounded set of successful object states. Exemplary sets are discussed in Sec. IV. An experiment in Sec. V shows repeatedly successful task executions based on the success sets. Section VI concludes the paper.

II. Relative Object Dynamics

In this section, we introduce transformations that allow for kinematic and differential object representations with respect to the end-effector frames. Furthermore, relevant physical models for gravitation and impacts are specified.

A. Kinematics and Differential Kinematics

Consider a n-DoF planar robot with an angle shaped end-effector as depicted in Fig. 2. Given that the robot dimensions are fixed, the end-effector position and orientation is entirely described by the vector of joint angles $\boldsymbol{q} = [q_1 \ \dots \ q_n]^{\mathrm{T}}$. The forward kinematic map is defined by the transformation matrix

$$\boldsymbol{T}_{\mathrm{e}}^{0}(\boldsymbol{q}) = \begin{bmatrix} \boldsymbol{R}_{\mathrm{e}}^{0}(\boldsymbol{q}) & \boldsymbol{o}_{\mathrm{e}}^{0}(\boldsymbol{q}) \\ \boldsymbol{0}^{\mathrm{T}} & 1 \end{bmatrix} , \tag{1}$$

where $\boldsymbol{R}_{\mathrm{e}}^{0}$ is a rotation matrix and $\boldsymbol{o}_{\mathrm{e}}^{0}$ is a translational vector. The inertial frame and the catching robot base frame

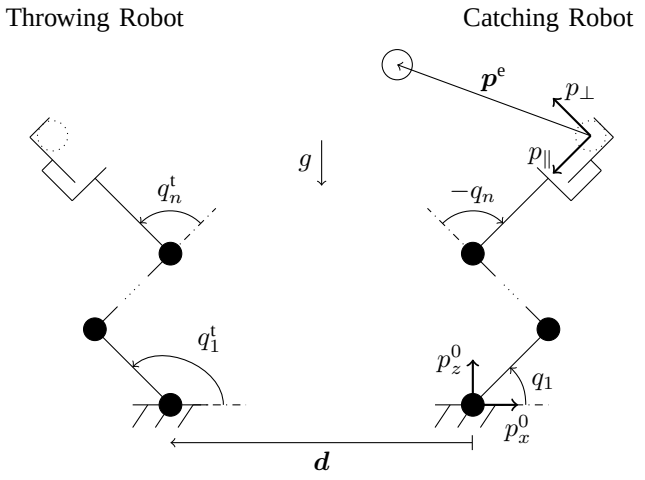

Fig. 2. Two symmetric planar robots with end-effector frames and relative object position.

coincide, cf. Fig. 2. The distance of the throwing robot from the catching robot is described by the vector $\boldsymbol{d}$. The inverse transformation is known as $\boldsymbol{T}_{0}^{\mathrm{e}}(\boldsymbol{q}) = (\boldsymbol{T}_{\mathrm{e}}^{0}(\boldsymbol{q}))^{-1}$. Thus, the position of an object with respect to the end-effector frame $\boldsymbol{p}^{\mathrm{e}}$ is calculated from the position in the reference frame $\boldsymbol{p}^{0}$ as

$$\tilde{\boldsymbol{p}}^{\mathrm{e}}(\boldsymbol{q}, \boldsymbol{p}^{0}) = \boldsymbol{T}_{0}^{\mathrm{e}}(\boldsymbol{q})\tilde{\boldsymbol{p}}^{0}, \tag{2}$$

with $\tilde{\boldsymbol{p}} = [\boldsymbol{p} \ 1]^{\mathrm{T}}$. The relative velocities and accelerations with respect to the end-effector frame of a flying object described in the base frame $(\boldsymbol{p}^{0}, \dot{\boldsymbol{p}}^{0}, \ddot{\boldsymbol{p}}^{0})$ and for a given manipulator catching motion $(\boldsymbol{q}, \dot{\boldsymbol{q}}, \ddot{\boldsymbol{q}})$ are

$$\dot{\boldsymbol{x}}^{\mathrm{e}} = \begin{bmatrix} \dot{\boldsymbol{p}}^{\mathrm{e}} & \ddot{\boldsymbol{p}}^{\mathrm{e}} \end{bmatrix}^{\mathrm{T}} = \begin{bmatrix} \boldsymbol{J}(\boldsymbol{q}, \boldsymbol{p}^{0})\dot{\boldsymbol{q}} + \boldsymbol{R}_{0}^{\mathrm{e}}(\boldsymbol{q})\dot{\boldsymbol{p}}^{0} \\ \boldsymbol{J}(\boldsymbol{q}, \boldsymbol{p}^{0})\ddot{\boldsymbol{q}} + \dot{\boldsymbol{J}}(\boldsymbol{q}, \dot{\boldsymbol{q}}, \boldsymbol{p}^{0}, \dot{\boldsymbol{p}}^{0})\dot{\boldsymbol{q}} + \boldsymbol{R}_{0}^{\mathrm{e}}(\boldsymbol{q})\ddot{\boldsymbol{p}}^{0} + \dot{\boldsymbol{R}}_{0}^{\mathrm{e}}(\boldsymbol{q}, \dot{\boldsymbol{q}})\dot{\boldsymbol{p}}^{0} \end{bmatrix}, \tag{3}$$

where the terms with the Jacobian $\boldsymbol{J}(\boldsymbol{q}, \boldsymbol{p}^{0}) = \frac{\partial \boldsymbol{p}^{\mathrm{e}}}{\partial \boldsymbol{q}}$ represent the relative dynamics due to the end-effector motion. The terms with the rotational matrix $\boldsymbol{R}_{0}^{\mathrm{e}}$ and its time derivative $\dot{\boldsymbol{R}}_{0}^{\mathrm{e}}$ add the object motion according to the end-effector orientation.

B. Relative Dynamic Contacts

If a catching motion $\boldsymbol{q}(t)$ is given, its time derivatives $\dot{\boldsymbol{q}}(t)$, $\ddot{\boldsymbol{q}}(t)$ are known. From here on, only the planar case is considered since all problems can be projected into the object flight plane. With transformations according to Fig. 2, the relative object position vector denotes as $\boldsymbol{p}^{\mathrm{e}} = [p_\perp \ p_\parallel]^{\mathrm{T}}$. Velocities $\dot{\boldsymbol{p}}^{\mathrm{e}} = [\dot{p}_\perp \ \dot{p}_\parallel]^{\mathrm{T}}$ and accelerations $\ddot{\boldsymbol{p}}^{\mathrm{e}} = [\ddot{p}_\perp \ \ddot{p}_\parallel]^{\mathrm{T}}$ are defined accordingly. In order to simplify the notation, the superscript is omitted for the parallel and perpendicular components in the catching end-effector frame.

For all calculations in this paper, a single collision model is introduced based on a rigid-body assumption for end-effector and object. From the detailed discussion on two-dimensional

rigid-body collisions in [10] and [11], we choose the case of a frictionless central collision. A frictionless collision treatment is already conservative because possibilities for energy dissipation are neglected. Hence, re-bounce heights calculated with the chosen model, mark a conservative upper bound. Fast rotating non-circular objects are an exception, which is typically avoided by robotic throws.

From the rigid-body assumption follows that collisions can be considered instantaneous as well as inelastic and are therefore fully described by a coefficient of restitution $0 < c_\mathrm{r} < 1$. For this coefficient of restitution, an upper bound must be found experimentally to be able to determine an upper bound for the re-bounce height. The post impact velocities of objects according to the frictionless model are given by

$$\dot{p}_\perp(t_\mathrm{c}^+) = -c_\mathrm{r}\dot{p}_\perp(t_\mathrm{c}^-)\ , \tag{4}$$

$$\dot{p}_\parallel(t_\mathrm{c}^+) = \dot{p}_\parallel(t_\mathrm{c}^-). \tag{5}$$

This reset of the object velocity $\dot{\boldsymbol{p}}^\mathrm{e}$ in the end-effector frame is analogous to a reset of the object velocity $\dot{\boldsymbol{p}}^0$ in the inertial frame, calculated by rearranging (3). Note that situations in which the Jacobian becomes singular need no consideration because rearranging the first line of (3) for $\dot{\boldsymbol{p}}^0$ does not require the inverse Jacobian.

III. Successful Nonprehensile Catching

A direct robotic catch describes the instantaneous establishment of continous contact between an object and an end-effector that were previously separated. It is most desirable to achieve a direct catch since it reduces the problem to find a single common state of object and end-effector. In case of nonprehensile catching, position and velocity are relevant states to avoid object re-bounce.

A. The Perfect Direct Catch

A perfect dynamic contact with a flat end-effector and an object happens at the distinct time instant t_c^*, at which the perpendicular components of the state $\boldsymbol{x}^\mathrm{e}$ are zero:

$$\boldsymbol{x}_\perp(t_\mathrm{c}^*) = \begin{bmatrix} p_\perp(t_\mathrm{c}^*) \\ \dot{p}_\perp(t_\mathrm{c}^*) \end{bmatrix} = \boldsymbol{0}. \tag{6}$$

In order to hit the catching end-effector of length $p_{\parallel,\max}$, the parallel component has to fulfill

$$0 \leq p_\parallel\,(t_\mathrm{c}^*) \leq p_{\parallel,\max} \tag{7}$$

at the same point in time.

For an infinitesimal short time instant t_c^- before t_c^*, two approach scenarios are possible, namely $p_\perp(t_\mathrm{c}^-) > 0$ and $p_\perp(t_\mathrm{c}^-) < 0$. With regard to the frame definition in Fig. 2, only the first scenario is reasonable. The latter statement is not feasible because the object would lie behind the end-effector in its direction of motion. Hence, in order to allow the object to approach the end-effector, the perpendicular constraint of negative velocity

$$\dot{p}_\perp(t_\mathrm{c}^-) < 0 \tag{8}$$

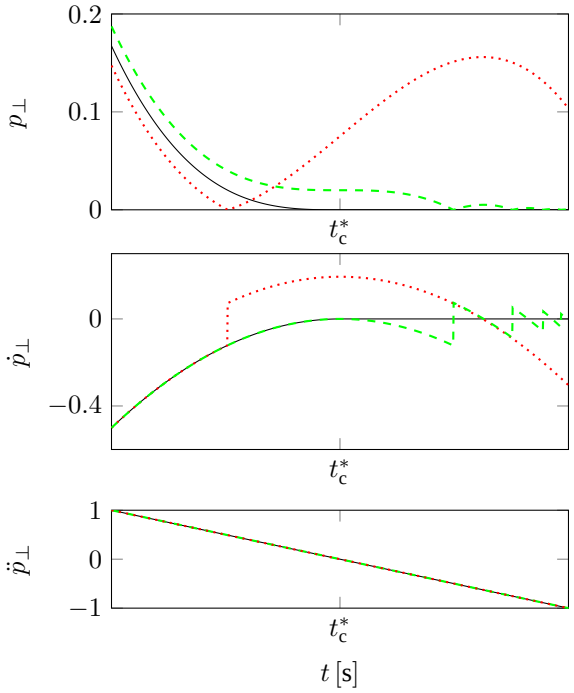

Fig. 3. Object trajectories for three academic contact scenarios in the end-effector coordinate frame: a perfect direct catch (solid), too early contact with undesireable large re-bounce (dotted), and a late contact with little and decreasing re-bounce (dashed). The relative acceleration is the same for all three scenarios, e.g. one dimensional object and end-effector motion.

must hold. In consideration of (6), this requires a positive relative perpendicular acceleration

$$\ddot{p}_\perp(t_\mathrm{c}^-) > 0. \tag{9}$$

The transition from a perfect dynamic contact to a perfect dynamic catch relies on a guaranteed negative perpendicular acceleration

$$\ddot{p}_\perp(t) < 0,\ \forall t > t_\mathrm{c}^*, \tag{10}$$

to ensure continuous contact. The solid lines in Fig. 3 depict such a perfect dynamic catch.

In practice however, it is difficult to achieve contact situations (6)-(10) reliably as they require an ideal object state. Any deviation from the desired object state most likely eliminates any possible solution t_c^* from (6). In case of early contacts, situations arise, where the relative post-impact acceleration $\ddot{p}_\perp(t_\mathrm{c}^+)$ is still positive, shown by the dotted lines in Fig. 3. The consequence is a large re-bounce that needs to be modeled until the next contact. Modelling such a long lasting re-bounce suffers from the typically imprecise knowledge of the coefficient of restitution c_r, which relates to an imprecise prediction of the post-impact velocity $\dot{p}_\perp(t_\mathrm{c}^+)$.

Impacts later than t_c^* are less problematic, as shown by the dashed lines in Fig. 3. Here, the re-bounce occurs during negative perpendicular acceleration, which has a limiting effect on the re-bounce height. Together with a coefficient of restitution $c_\mathrm{r} < 1$, the re-bounce height is strictly monotonically decreasing. Too late contacts however, must deal

with high relative velocities and thus again with larger re-bounces.

B. The Successful Quasi-Direct Catch

Due to the unique solution of a perfect direct catch and in the presence of uncertain object states, re-bouncing contacts are inevitable. In order to provide successful catching for a whole set of initial contact states, the two major results from the previous discussion are considered. Firstly, contacts with positive perpendicular acceleration must be prevented. Secondly, if negative perpendicular acceleration can be guaranteed between multiple contacts, the re-bounce height decreases strictly monotonically. Consequently, an initial contact can establish continuous contact successfully if negative perpendicular acceleration is guaranteed during all re-bounces. This is what we define as a *quasi-direct* catch.

For an explicit discussion on the re-bounce height a maximum negative perpendicular acceleration constraint $\ddot{p}_{\perp,\max}$ is introduced as

$$\ddot{p}_{\perp}(t, \boldsymbol{p}^{\mathrm{e}}, \dot{\boldsymbol{p}}^{\mathrm{e}}) < \ddot{p}_{\perp,\max} < 0 \ . \tag{11}$$

This constraint must hold for all possible object velocities after contact until the end-effector comes to rest. Due to the dependencies of $\ddot{p}_{\perp}$ on the relative position $\boldsymbol{p}^{\mathrm{e}}$ and velocity $\dot{\boldsymbol{p}}^{\mathrm{e}}$ of the object, the constraint can only be shown to hold for a restricted set of relative object states. Therefore, a success area $\mathcal{S}$ is defined originating from the end-effector design. This area should never be left by the object after a successful initial contact. The upper acceleration bound can then be defined as

$$\begin{aligned}\ddot{p}_{\perp,\max} = \max\{\ddot{p}_{\perp}(t, \boldsymbol{p}^{\mathrm{e}}, \dot{\boldsymbol{p}}^{\mathrm{e}}) \mid t \in [\,t_{\mathrm{d}}, t_{\mathrm{f}}\,] \wedge \\ \boldsymbol{x}^{\mathrm{e}} \in \mathcal{S} \ \wedge \ \boldsymbol{x}^{\mathrm{e}} \in \mathcal{V})\} \ ,\end{aligned} \tag{12}$$

where the velocity set $\mathcal{V}$ needs to be chosen according to (11). The time instant t_{d} specifies the start of an arbitrary decelerating catching motion. The time instant t_{f} denotes the end of the catching motion where the end-effector comes to rest. The acceleration of the catching end-effector is not regarded here.

From (4) and (11)-(12) it follows that the maximum re-bounce distance is strictly monotonically decreasing with every cycle. Hence, once the perpendicular relative velocity after initial contact $\dot{p}_{\perp}(t^{+})$ is lower than some upper bound $\dot{p}_{\perp,\max} > 0$, the trial can be labeled successful.

In this work, $\dot{p}_{\perp,\max}$ is calculated based on the worst case which is the assumption of a guaranteed constant negative acceleration of at least $\ddot{p}_{\perp,\max}$ after t_{d}. This allows for linear time treatment of

$$t_{\mathrm{rb}} = \frac{\dot{p}_{\perp}(t_{\mathrm{c}}^{+})}{-\ddot{p}_{\perp,\max}} = \frac{-c_{\mathrm{r}}\dot{p}_{\perp}(t_{\mathrm{c}}^{-})}{-\ddot{p}_{\perp,\max}} \ , \tag{13}$$

which is the worst case duration of positive post-impact velocities. The maximum re-bounce height h_{r} can thus be calculated by

$$\begin{aligned}h_{\mathrm{r}} &= -c_{\mathrm{r}}\dot{p}_{\perp}(t_{\mathrm{c}}^{-})t_{\mathrm{rb}} + \tfrac{1}{2}\ddot{p}_{\perp,\max}{t_{\mathrm{rb}}}^{2} \\ &= \frac{{c_{\mathrm{r}}}^{2}\dot{p}_{\perp}^{2}(t_{\mathrm{c}}^{-})}{-\ddot{p}_{\perp,\max}} + \frac{{c_{\mathrm{r}}}^{2}\dot{p}_{\perp}^{2}(t_{\mathrm{c}}^{-})}{2\ddot{p}_{\perp,\max}} = \frac{{c_{\mathrm{r}}}^{2}\dot{p}_{\perp}^{2}(t_{\mathrm{c}}^{-})}{-2\ddot{p}_{\perp,\max}} \ ,\end{aligned} \tag{14}$$

which is the well-known free flight parabola with $p_{\perp}(t_{\mathrm{c}}) = 0$. Rearranging leads to the negative bounded velocity range

$$\dot{p}_{\perp,\mathrm{lb}} = -\frac{\sqrt{-2\ddot{p}_{\perp,\max}h_{\mathrm{r}}}}{c_{\mathrm{r}}} < \dot{p}_{\perp}(t_{\mathrm{c}}^{-}) < 0 \ , \tag{15}$$

whereas h_{r} depends on the end-effector design and $\ddot{p}_{\perp,\max}$ is a design parameter. The positive solution of $\dot{p}_{\perp}(t_{\mathrm{c}}^{-})$ to (14) would result in a negative t_{rb} due to (13) and is thus not feasible. In combination with a rearranged (3), it is now possible to calculate bounds for $\dot{\boldsymbol{p}}^{0}(t)$ which result in successful catches. Note that c_{r} is a considerable source of uncertainty here.

C. Sets of Successful Object States

With the above discussion, it is now possible to define a set of object states that lead to successful quasi-direct catching. For this purpose, a sampled robot catching motion $\boldsymbol{q}(t_k)$ is regarded. For each time step $t_k \in [t_{\mathrm{d}}, t_{\mathrm{f}}]$ of the robot catching motion, a set of object states

$$\mathcal{X}_k(t_k) = \{\boldsymbol{x}_k \mid \boldsymbol{H}_k\boldsymbol{x}_k \leq \boldsymbol{b}_k \wedge \boldsymbol{E}_k\boldsymbol{x}_k = \boldsymbol{g}_k\} \tag{16}$$

can be defined based on the previous discussion. The entries of the matrix $\boldsymbol{H}_k$ and the vector $\boldsymbol{b}_k$ formulate a set of half spaces that serve as multi-dimensional inequality constraints, while $\boldsymbol{E}_k$ and $\boldsymbol{g}_k$ formulate equality constraints. The unity of these constraints results in a polytope for every time step t_k, each with a bounded set of successful contact states.

In order to express the the set of object states at an arbitrary point in time, reachable set computations are used. Since the free object flight is an autonomous linear affine dynamic, we define the reachable set similar to [14] as

$$\mathcal{X}_k(t) = Reach(\mathcal{X}_k(t_k), t). \tag{17}$$

For multiple consecutive sets, their intersection is always empty: $\mathcal{X}_i(t) \cap \mathcal{X}_j(t) = \emptyset, \ \forall i \neq j$. This is due to the presence of at least one equality constraint for the precise contact at a certain point in time t_k.

IV. Simulation and Numerical Solution

For the evaluation and discussion of the previously introduced sets, we consider two planar symmetric robot arms, each with $n = 2$ revolute joints. The link lengths l_1 and l_2 are listed in Tab. I. The choice of this setup is additionally challenging as position and orientation of the end-effector are coupled. Thus, the higher the velocities required for the dynamic catch, the shorter the time becomes in which the robot can match an object's flight trajectory.

TABLE I

Kinematic dimensions and parameters.

$\lvert\boldsymbol{d}\rvert$ [m]	l_1 [m]	l_2 [m]	$p_{\parallel,\max}$ [m]	h_{r} [m]
1.12	0.32	0.345	0.035	0.005

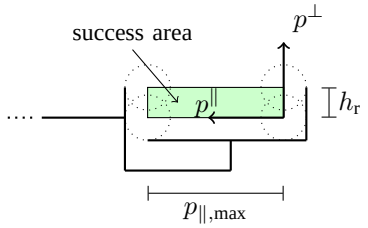

Fig. 4. End-effector success area for which a velocity set is searched such that an object (ball) never leaves this area again.

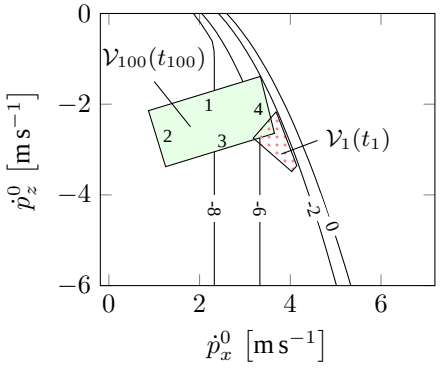

Fig. 5. The isolines mark the top right bound of set $\mathcal{V}$ in (19) for examplary values $\ddot{p}_{\perp,\max}$. Additionally, two example sets $\mathcal{V}_1(t_1)$ (dotted) and $\mathcal{V}_{100}(t_{100})$ (filled) are plotted for $\ddot{p}_{\perp,\max} = -2$. The run of the isolines highly depends on the definition of the success area in Fig. 4 and the catching motion.

A. Verification of Constraints and Assumptions

Primarily, it has to be verified that (8) holds throughout the catching phase. For the regarded catching motion, this already holds by design. The angular velocities of the catching robot $\dot{\boldsymbol{q}}$ is always smaller than the throwing motion $\dot{\boldsymbol{q}}^{\mathrm{t}}$ at the object release instant t_r and the desired contacts lie lower: $p_\mathrm{z}^0(t) < p_\mathrm{z}^0(t_\mathrm{r})$, $\forall t \in [t_\mathrm{d}, t_\mathrm{f}]$.

An intermediate step is necessary to find the upper perpendicular acceleration bound $\ddot{p}_{\perp,\max}$ based on (12) because $\ddot{p}_\perp$ depends on the object position $\boldsymbol{p}^0$ and velocity $\dot{\boldsymbol{p}}^0$. In order to find a viable set of the velocity vector for which $\ddot{p}_{\perp,\max}$ holds, the further discussion is limited to a success area

$$\mathcal{S} = \left\{ \boldsymbol{x}^0 \,|\, \boldsymbol{p}^\mathrm{e} \in [0, h_\mathrm{r}] \times [0, p_{\parallel,\max}] \right\} , \tag{18}$$

which is marked in Fig. 4. This restriction is possible if the choice of $\mathcal{V}$ in (12) ensures that the object never leaves this area again after an initial contact. The velocity set in (12) is then

$$\mathcal{V} = \left\{ \boldsymbol{x}^0 \,|\, \ddot{p}_\perp(t, \boldsymbol{p}^\mathrm{e}, \dot{\boldsymbol{p}}^\mathrm{e}) < \ddot{p}_{\perp,\max} \; \forall \boldsymbol{x}^0 \in \mathcal{S} \wedge t \in [t_\mathrm{d}, t_\mathrm{f}] \right\} . \tag{19}$$

The simulation results of this set for a given catching motion are shown in Fig. 5. The isolines illustrate the upper border of $\mathcal{V}$ for a choice of $\ddot{p}_{\perp,\max}$. This upper acceleration bound in the velocity space is guaranteed for all object positions $\mathcal{S}$ during the entire catching period $t \in [t_\mathrm{d}, t_\mathrm{f}]$. From (18) and (19), it can further be concluded that the shapes of these isolines highly depend on the success area definition and the catching motion.

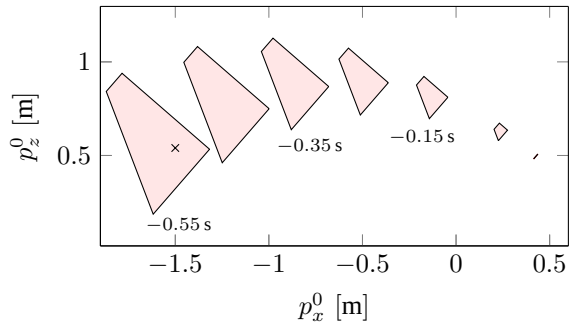

Fig. 6. Object positions $\mathcal{C}_1(t)$ at multiple points in time before t_d that lead to a successful catch. If the object velocity at t lies in the according set $\mathcal{V}_1(t)$, the trial is successful. The cross marks a position for which the velocity solution sets are discussed.

B. Successful Sets

After validating the assumption, the sets $\mathcal{X}_k(t_k)$ that lead to a successful catch can be found for every time step $t_k \in [t_\mathrm{d}, t_\mathrm{f}]$ of the robot catching motion. For this purpose, only contact situations $p_\perp = 0$ in the success area are considered, represented by the set

$$\mathcal{C}_k(t_k) = \left\{ \boldsymbol{x}^0(t_k) \,|\, \boldsymbol{x}^0 \in \mathcal{S} \wedge p_\perp = 0 \right\} . \tag{20}$$

For these positions, a prior-impact velocity subset of $\mathcal{V}$ for every time step t_k^- is defined as

$$\mathcal{V}_k^-(t_k^-) = \left\{ \boldsymbol{x}^0(t_k^-) \,|\, \dot{p}_\perp \in [\dot{p}_{\perp,\mathrm{lb}}, 0] \; \forall p_\parallel \in [0, p_{\parallel,\max}] \right. \\ \left. \wedge \dot{p}_\parallel < 0 \wedge \boldsymbol{x}^0(t_k^-) \in \mathcal{V} \right\} . \tag{21}$$

This definition ensures that all prior-impact velocities fullfil (15) independently of the contact position in the success area. In Fig. 5 this produces the boundaries 1 and 3 for $\dot{p}_\perp = 0$ and $\dot{p}_\perp = \dot{p}_{\perp,\mathrm{lb}}$, respectively. Major dependencies of $\dot{p}_{\perp,\mathrm{lb}}$ from (15) are the coefficient of restitution c_r, the maximum desired re-bounce height h_r, and the maximum negative velocity $\ddot{p}_{\perp,\max}$. In order to avoid disadvantageous contacts with the end-effector edge at $p_\parallel = p_{\parallel,\max}$, we choose the parallel velocity $\dot{p}_\parallel$ to be negative, represented by boundary 2. Additionally, it must be ensured that (11) holds also for post-impact velocities leading to the set

$$\mathcal{V}_k(t_k) = \left\{ \boldsymbol{x}^0(t_k) \,|\, \boldsymbol{x}^0(t_k^-) \in \mathcal{V}_k^- \wedge \boldsymbol{x}^0(t_k^+) \in \mathcal{V} \right\} , \tag{22}$$

represented by boundary 4.

According to the model assumptions made, the set of states that lead to successful catching can now be formulated as the intersection

$$\mathcal{X}_k(t_k) = \mathcal{C}_k(t_k) \cap \mathcal{V}_k(t_k). \tag{23}$$

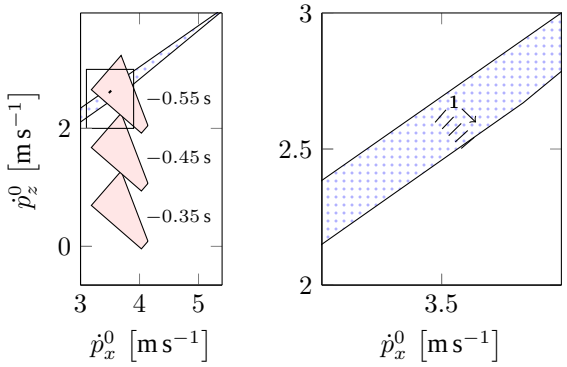

Fig. 7. **Left:** Object velocities $\mathcal{V}_1(t)$ at multiple points in time before t_d that may lead to a successful catch (filled). The dot in the filled area shows the set of successful object velocities at $t = t_\mathrm{d} - 0.55\,\mathrm{s}$ for the position marked in Fig. 6. The dotted area indicates possible release velocities of the robot in use for this position and joint configuration. **Right:** A zoom of valid release velocities from $k = 1$ to $k = 21$ in steps of five for the same point in time t.

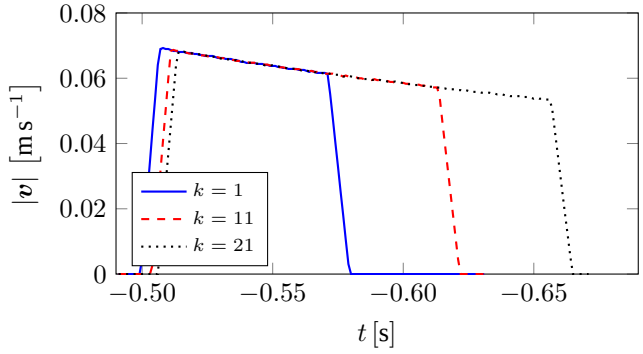

Fig. 8. The one-dimensional set length of $\mathcal{V}_k(t)$ for the position marked in Fig. 6 over time t. The longer the flight time until impact, the smaller the velocity set size. When the fixed position reaches the edge of $\mathcal{C}_k(t)$ the size of $\mathcal{V}_k(t)$ goes down to zero.

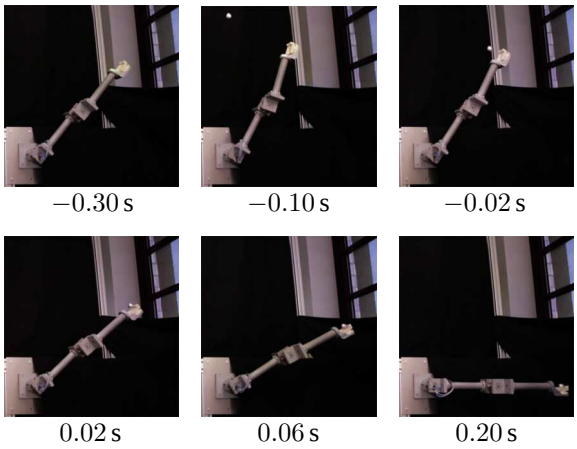

Fig. 9. Frames of the catching experiment with $t_\mathrm{d} = 0\,\mathrm{s}$.

C. Discussion of Results

The result of the success analysis is presented with Figs. 6 and 7. The first plot shows potentially successful object states at different points in time as a projection of $\mathcal{X}_k(t)$ onto the position dimensions. It can be interpreted such that for every time-position combination within the sets, there exists a corresponding one dimensional set of velocities that leads to a successful catch. For further reference we denote the length of this one dimensional solution set as $|\boldsymbol{v}|$. One possibility to calculate $\boldsymbol{v}$ is to take the difference of the first and the last velocity vector $\dot{\boldsymbol{p}}^0(t)$ that is in the velocity set $\mathcal{V}_k(t)$ given a position $\boldsymbol{p}^0(t)$.

If the position $\boldsymbol{p}^0$, the time t and the catching step k are fixed, the length $|\boldsymbol{v}|$ is only influenced by the size of the catching surface defined in (7). The chosen release position does not directly influence the size of the velocity solution set. The zoomed plot on the right hand side in Fig. 7 illustrates valid velocities for consecutive steps k of the sampled catching motion.

The only parameter that does have an influence on the size of $\mathcal{V}_k(t)$ is the timing, more precisely the time until impact. As Fig. 8 shows, the velocity set size increases if the time until impact is reduced. For a given position and a particular catching step k, this can be done by changing t in $\mathcal{X}_k(t)$ until the position is close to the set border. Figure 8 shows this size for $k = 1$ at several points in time t. If the chosen position is too close to the boundary of its set, the respective velocity set size is reduced to zero. Consequently, the choice of the position influences the velocity set size indirectly by the time range that can possibly be covered. However, the maximum velocity set size is not the best choice since in turn the amount of valid catching sets k for the position-time combination would be reduced.

V. Experiment

For the experimental evaluation, two symmetric serial manipulators with end-effectors moving in a vertical plane were built. Each of the manipulators is driven by two PD-controlled revolute joints based on angular displacement sensing with resolution $1.5 \times 10^{-5}\,\mathrm{rad}$. Angular velocities are based on numerical differentiation of the angular displacement with resolution $1.5 \times 10^{-2}\,\mathrm{rad\,s^{-1}}$ considering the time sampling in steps of $0.001\,\mathrm{s}$. Every joint is actuated with a $150\,\mathrm{W}$ Maxon motor attached to a 1:100 Harmonic Drive gear. The maximum possible joint velocities are $7\,\mathrm{rad\,s^{-1}}$ on the load side. The distance $|\boldsymbol{d}|$ between the two robot bases and the kinematic dimensions are given in Tab. I.

Each of the two robots is able to perform both tasks throwing and catching with the same end-effector. An exemplary catching motion is given and performs open-loop without knowledge of the current object state, cf. Fig. 9. For this motion, successful object states were defined and calculated in Sec. IV. From the set of successful object states, one object state is chosen which is not close to any bounds of the success set. Furthermore, this one object state is amongst the reachable end-effector states of the throwing robot, depicted in Fig. 7 by the dotted area. Considering possible release and catching positions, the overall open-loop flight distance is about $1.8\,\mathrm{m}$.

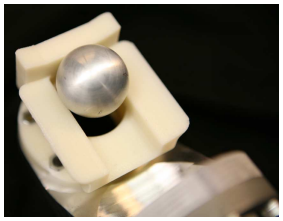

Fig. 10. End-effector for throwing and catching spherical objects in a vertical plane. The middle track minimizes the contact surface whilst keeping the object at a defined position for throwing. Inclined side planes increase the catching area.

The plastic end-effector shown in Fig. 10 is particularly designed for planar throwing and catching of spherical objects, here an aluminum ball with radius $1.5\,\mathrm{cm}$ and thus negligible aerodynamic drag. The planar surfaces, left and right of the middle track, are slightly inclined towards the middle. This directs the object back into the vertical plane during the catch if distortions in the direction of the non-actuated dimension appear. In the center, the end-effector provides 3-point contact to minimize the contact surface and to fix the object in the vertical plane for (re-)throwing.

Experimental results verify the discussion of the successful object states with 18 successful catches out of 20. The attached video shows one of the successful throwing and catching cycles. Furthermore, it illustrates what happens in case of undesirable early contacts as they were described in Sec. III.

The release configuration on the throwing side is chosen such that a sufficient range of release velocities is available and such that the absolute velocity is sufficiently high. The configuration $q_1^\mathrm{t} = 0.175\,\mathrm{rad}$ and $q_1^\mathrm{t} = 2.094\,\mathrm{rad}$ has shown to be a good trade-off, cf. Fig. 2. For similar desired release velocities, these angles cannot be chosen much larger as the motors already operate close to their power limits. The resulting release position is $p_x^0 = -1.5\,\mathrm{m}$ and $p_z^0 = 0.54\,\mathrm{m}$, which is also marked by a cross in Fig. 6.

On the throwing side, limiting effects on the task success originate in release state inaccuracies that are larger than the currently found success sets. On the catching side, the so far heuristically chosen catching motion contains unused potential. For example, the catching motion could be re-planned by using the presented method.

VI. Conclusion and Future Work

In this work, quasi-direct catching has been proposed as an effective way to deal with uncertain object states as a set of potentially successful object states becomes available. It was explained how these sets of successful object states can be calculated efficiently for given catching motions at any point in time before contact. The time until contact has been identified as the most crucial and complex parameter for which generalized statements cannot be made.

The flexibility of the implementation enables intense cause and effect discussions on all relevant constraints and parameters beyond this work. The representations can be extended to additional degrees of freedom like object orientation and rotational velocity. For such extensions, the physical model needs further attention in terms of a range of successful contacts. The set description and calculation scales well for this purpose unless nonlinear models for free object flight are considered.

In future work, the algorithm will be enhanced to also consider undesirable contacts, e.g. when the object trajectory crosses parts of the accelerating robot motion. In the sequel, it will be possible to investigate and improve the catching trajectory itself jointly with the end-effector design.

Acknowledgment

The authors would like to thank Alexander Pekarovskiy for his contribution to the experimental setup.

References

[1] M. T. Mason and K. Lynch, "Dynamic manipulation," in *Proc. of the IEEE/RSJ Int. Conf. on Intelligent Robots and Systems*, vol. 1, July 1993, pp. 152–159.

[2] K. M. Lynch and M. T. Mason, "Dynamic Nonprehensile Manipulation: Controllability, Planning, and Experiments," *The International Journal of Robotics Research*, vol. 18, no. 1, pp. 64–92, 1999.

[3] G. Bätz, A. Yaqub, H. Wu, K. Kuhnlenz, D. Wollherr, and M. Buss, "Dynamic manipulation: Nonprehensile ball catching," in *18th Mediterranean Conference on Control Automation*, June 2010, pp. 365–370.

[4] A. Pekarovskiy, F. Stockmann, M. Okada, and M. Buss, "Hierarchical robustness approach for nonprehensile catching of rigid objects," in *Proc. of the IEEE/RSJ Int. Conf. on Intelligent Robots and Systems*, Sept. 2014, pp. 3649–3654.

[5] B. Hove and J.-J. Slotine, "Experiments in robotic catching," in *Proc. of the American Control Conference*, June 1991, pp. 380–386.

[6] J. Kober, M. Glisson, and M. Mistry, "Playing catch and juggling with a humanoid robot," in *Proc. of the 12th IEEE-RAS Int. Conf. on Humanoid Robots*, Nov. 2012, pp. 875–881.

[7] E. Croft, R. Fenton, and B. Benhabib, "Optimal rendezvous-point selection for robotic interception of moving objects," *IEEE Trans. Syst., Man, Cybern. B*, vol. 28, no. 2, pp. 192–204, Apr. 1998.

[8] B. Bäuml, T. Wimböck, and G. Hirzinger, "Kinematically optimal catching a flying ball with a hand-arm-system," in *Proc. of the IEEE/RSJ Int. Conf. on Intelligent Robots and Systems*, Oct. 2010, pp. 2592–2599.

[9] A. Pekarovskiy and M. Buss, "Optimal control goal manifolds for planar nonprehensile throwing," in *Proc. of the IEEE/RSJ Int. Conf. on Intelligent Robots and Systems*, Nov. 2013, pp. 4518–4524.

[10] Y. Wang and M. T. Mason, "Modeling impact dynamics for robotic operations," in *Proc. of the IEEE Int. Conf. on Robotics and Automation*, vol. 4, Mar. 1987, pp. 678–685.

[11] ——, "Two-Dimensional Rigid-Body Collisions With Friction," *Journal of Applied Mechanics*, vol. 59, no. 3, pp. 635–642, 1992.

[12] J. E. Routh, *Dynamics of a system of rigid bodies*. New York: Dover, 1960.

[13] S. Schaal and C. Atkeson, "Open loop stable control strategies for robot juggling," in *Proc. of the IEEE Int. Conf. on Robotics and Automation*, vol. 3, May 1993, pp. 913–918.

[14] Z. Han and B. H. Krogh, "Reachability analysis of large-scale affine systems using low-dimensional polytopes," in *Hybrid Systems: Computation and Control*. Springer, 2006, pp. 287–301.